



Repositorio Institucional de la Universidad Autónoma de Madrid

<https://repositorio.uam.es>

Esta es la **versión de autor** del artículo publicado en:
This is an **author produced version** of a paper published in:

Nanoscale 10.47 (2018): 22400-22408

DOI: <https://doi.org/10.1039/C8NR08438F>

Copyright: © The Royal Society of Chemistry 2018

El acceso a la versión del editor puede requerir la suscripción del recurso

Access to the published version may require subscription

Synergy of light harvesting and energy transfer as well as short-range charge shift reactions in multicomponent conjugates

Ettore Fazio,^a Kim A. Winterfeld,^b A. López-Pérez,^a Tomás Torres^{*a,c,d} Dirk M. Guldi,^{*b} Gema de la Torre^{*a,c}

We report herein on the design, the synthesis, and the characterization of a panchromatic, charge stabilizing electron donor-acceptor conjugate: (BBPA)₃-ZnPc-ZnPor-SubPc **1**. Each component, that is, bis(biphenyl)phenylamine (BBPA), Zn(II) porphyrin (ZnPc), Zn(II) phthalocyanine ZnPc, and subphthalocyanine (SubPc), has been carefully chosen and modified to enable a cascade of energy and charge transfer processes. On one hand, ZnPc, has been functionalized with three electron-donating BBPA as primary and secondary electron donors and to stabilize the final charge-separated state, and, on the other hand, a perfluorinated SubPc has been selected as ultimate electron acceptor. In addition, the ZnPc unit contains several trifluoromethylphenyl moieties to match its energy levels to those of the other components. In fact, irradiation of the heteroarray **1** triggers a cascade of light harvesting across the entire visible range, unidirectional energy transfer, exergonic charge separating, and short-range charge shifting to afford in 14% quantum yield a (BBPA)₃⁺⁺-ZnPc-ZnPor-SubPc⁻ charge-separated state. The lifetime of the latter reaches well into the range of tens of nanoseconds.

Introduction

The success of the photosynthetic process in converting sunlight into chemical energy relies on the synergy of the efficient absorption of light, the transduction of excitation energy, and the cascade of unidirectional charge transfer reactions. It is the latter that ultimately leads to the synthesis of carbohydrates.¹ Interdisciplinary efforts have been driven by the notion to understand the mechanism of light conversion in the photosynthetic systems.² The overarching goal is the design of artificial architectures with an optimized light absorption, on one hand, and a slow-down of charge recombination, on the other hand. Failure to any of the above leads to an inefficient conversion of sunlight. To this end, a palette of artificial photosynthetic architectures, in which individual components have been adequately tailored and spatially arranged, and in which light absorption and charge recombination have been designed and optimized, are at the forefront of investigations.^{3,4} Multi-component systems in the form of molecular triads, tetrads, etc. – similar to what is known from the natural system – enable cascades of mediating not only energy but also charges along the different components. Of great relevance is the

stepwise charge transfer along the components as it enables the spatial separation of charges and, as such, the suppression of the undesired recombination of charges.

Porphyrinoids are among the most widely used chromophores in artificial photosynthetic architectures. Largely, this is due to their strong and tunable optical absorption as well as their rich redox chemistry. Most notably, porphyrins (Por) have been incorporated into multicomponent conjugates as either light harvesting and/or electron donors.⁵⁻¹³ Phthalocyanines¹⁴⁻¹⁷ (Pc) and subphthalocyanines (SubPc)^{18,19} serve similarly as light- and redox-active components. All of the aforementioned chromophores have a broad synthetic versatility that allows for easy modulation of their electronic character. Moreover, Por, SubPc, and Pc with their maximum absorption at 400, 500, and 700 nm, respectively, complement each other and, in turn, absorb throughout most of the visible and near-infrared section of the solar spectrum.

Covalent and non-covalent means have been employed to combine these porphyrinoids and to afford a broad palette of different heteroarrays.²⁰⁻²³ In particular, a number of simple Por-Pc and Pc-SubPc conjugates have been targeted and studied within the context of generating charge-separated states upon photoexcitation. More sophisticated, on one hand, and more resourceful, on the other hand, are multichromophoric combinations of Pors with either Pcs^{24,25} or SubPcs²⁶ and other electroactive units. For example, our group has reported on a few leading examples of ZnPc-C₆₀-Por and ZnPc-(Por)₂-(C₆₀)₂ arrays.²⁷ A sequence of energy and charge transfer reactions commences with the photoexcitation of the ZnPors in these arrays, and the ZnPcs acting as energy funnels. Notable is, however, the fact that the ZnPcs are not placed at the center. The number of examples, in which Pcs are placed at

^a Departamento de Química Orgánica, Universidad Autónoma de Madrid, C/ Francisco Tomás y Valiente 7, 28049-Madrid,

^b Department of Chemistry and Pharmacy, Interdisciplinary Center for Molecular Materials (ICMM), Friedrich-Alexander-Universität Erlangen-Nürnberg, Egerlandstr. 3, 91058 Erlangen, Germany

^c Institute for Advanced Research in Chemical Sciences (IAdChem), Universidad Autónoma de Madrid, 28049 Madrid, Spain

^d IMDEA Nanociencia, C/Faraday, 9, Cantoblanco, 28049 Madrid, Spain.

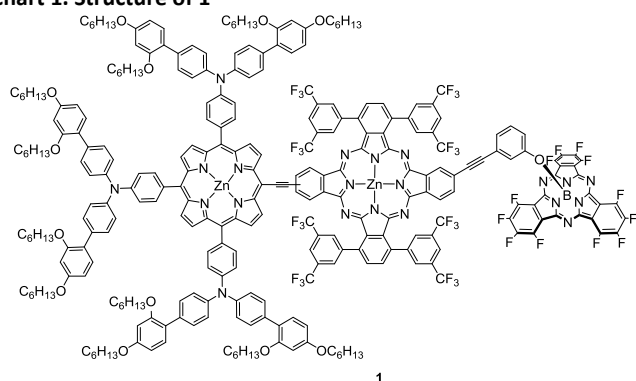
Electronic Supplementary Information (ESI) available: [details of any supplementary information available should be included here]. See DOI: 10.1039/x0xx00000x

the center, are rare and limited to the assembly of metal-ligand axial coordination at the Pc.^{28–31}

Here, we report on the synthesis of a panchromatic, charge stabilizing (BBPA)₃–ZnPc–ZnPor–SubPc array (BBPA stands for bis(biphenyl)phenylamine) (Chart 1) and its full-fledged photophysical characterization. We are aware of just a single report regarding related multichromophoric Pc–Por–SubPc ensembles, in which non-covalent interactions were used to bring the individual components together.³² In other words, **1** is the first fully covalent array containing all three chromophores, and also the first covalent conjugate comprising a Pc located as central unit of the ensemble. Please note that each component in **1** has been tailored towards an appropriate energy level alignment to support a cascade of energy and charge transfer processes. Firstly, the electron-donating ZnPor has been functionalized with three BBPA as primary and secondary electron donors and to stabilize the final charge-separated state.³³ Secondly, a perfluorinated SubPc has been selected owing to the fact that it is a strong electron acceptor with a low-energy LUMO.^{34,35} Thirdly, ZnPc contains several trifluoromethylphenyl moieties to match its energy levels to those of the other components.

In short, we expect from our careful design of (BBPA)₃–ZnPc–ZnPor–SubPc **1** a photosynthetic reaction center mimic giving rise to a long-lived charge-separated state, of which the formation is based on the synergy of light harvesting, energy transfer, charge separation, and charge shift.

Chart 1. Structure of 1



Experimental section

Synthesis and Characterization. A full account of the synthesis and characterization of all new compounds, together with detailed reaction schemes, is provided in the Supporting Information.

Femtosecond Time-Resolved Transient Absorption Spectroscopy. Transient absorption spectroscopy (TAS) in the femto- to microsecond regime was carried out using a transient absorption pump/probe HELIOS/EOS system in combination with an amplified CPA-2110 Ti:sapphire laser (Clark MXR: 1 kHz, 150 fs pulse width, 775 nm output). The excitation wavelength of 676 nm was generated with a non-collinear optical parameter amplifier (NOPA, Clark MXR). All measurements were conducted under argon atmosphere.

The data were fitted by multiwavelength analysis with Origin (OriginLab, Northampton, MA) as well as global target analyses. The latter were performed with the opensource software package GloTarAn, a Java based graphical user interface to the R-package TIMP.^{36,37} The wavelength-dependent character (dispersion) of the instrument response function was modelled and taken into account.

Electrochemistry. Cyclic voltammetry and square wave voltammetry measurements were performed on an Autolab PGStat 30 equipment using a three-electrode configuration system. The measurements were carried out using dry CH₂Cl₂ solutions containing 0.1 M tetrabutylammonium hexafluorophosphate (TBAPF₆) and a concentration of approximately 10^{−4} M of the corresponding compound. A glassy carbon electrode (3 mm diameter) was used as the working electrode, and a platinum wire and an Ag/AgNO₃ (in CH₃CN) electrode were employed as the counter and the reference electrodes, respectively. Ferrocene (Fc) was used as an internal reference and all the potentials were given relative to the Fc/Fc⁺ couple. Scan rate was 100 mVs^{−1} unless otherwise specified. The E^{1/2} values were extracted from square wave measurements.

UV–Vis Absorption and Fluorescence Spectroscopy. Steady-State absorption spectra between 300 and 900 nm were obtained with a PerkinElmer Lambda 2 dual beam absorption spectrometer. Steady-state fluorescence spectra were recorded with a Horiba FluoroMax3 spectrometer in the visible detection range. For determination of fluorescence quantum yields by the comparative method, the OD at the wavelength of excitation and beyond was kept below 0.1.

Results and discussion

Synthesis. The preparation of **1** started with the synthesis of the individual components (Scheme 1). (BBPA)₃–ZnPc **2**, featuring three BBPA moieties and an ethynyl group was synthesized via statistical condensation of 4-(bis(2',4'-bis(hexyloxy)-[1,1'-biphenyl]-4-yl)amino)benzaldehyde **3**,³⁸ 3-(trimethylsilyl)-2-propynal, and pyrrole, following Lindsey conditions.^{39,40} The obtained free-base Por **4** was metallated with Zn(OAc)₂ ((BBPA)₃–ZnPc **5**), and deprotected with TBAF to yield the corresponding (BBPA)₃–ZnPc **2**. Diiodo-containing ZnPc **6** and F₁₂SubPc **7** were prepared following procedures described in our group.^{41,42}

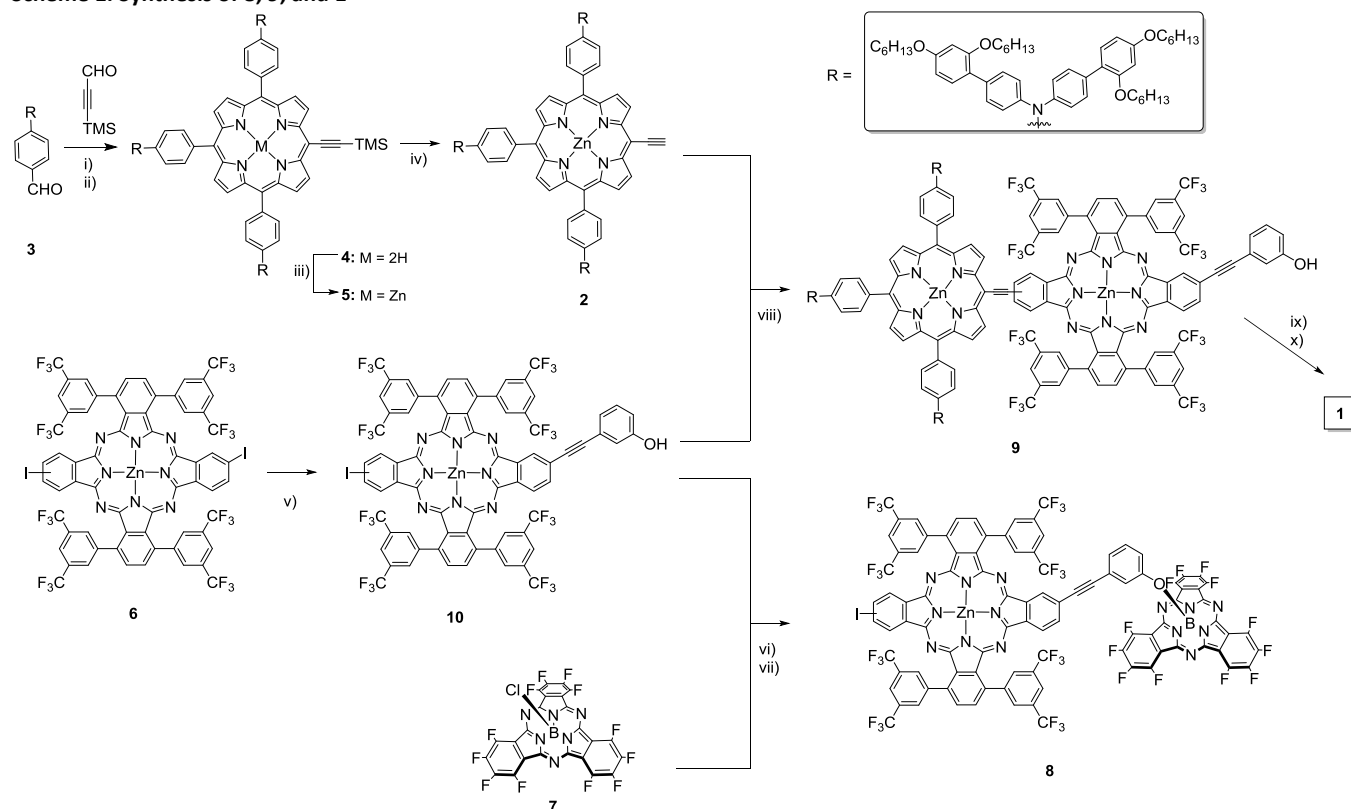
Next, we assembled the three porphyrinoids into target **1**. During the synthetic process, we prepared **8** and **9** as important references for gathering comprehensive insights into the photophysics of **1**. Sonogashira reaction of diiodo ZnPc **6** with 3-ethynylphenol afforded the intermediate ZnPc **10**, which was further converted into ZnPc–SubPc **8**. The latter reaction involved a substitution of the chlorine atom at the axial position of F₁₂SubPc **7** by the phenol group in **10**, which was carried out following a one-pot, two-step methodology developed in our group.⁴³ For the preparation of (BBPA)₃–ZnPc–ZnPor **9**, we performed a Sonogashira coupling of ZnPc **6** with deprotected (BBPA)₃–ZnPc **2**. Here, copper-free conditions were necessary to avoid the formation of ZnPor–ZnPc homocoupling products.

Finally, the target compound **1** was obtained from F₁₂SubPc **7** and (BBPA)₃-ZnPor-ZnPc **9**, following the SubPc axial substitution protocol described for the synthesis of ZnPc-SubPc **8**. Notably, **1** and references **8**, **9** are mixtures of two regioisomers, since the starting diiodo **6** was also a mixture of *syn* and *anti* isomers, which could not be separated.⁴⁴

All structures were unequivocally confirmed by means of HR-MALDI-TOF mass spectrometry, UV-vis, and NMR spectroscopy (see Supporting Information, Figures S1-S13). In Figures 1 and S1, the ¹H-NMR spectrum of **1** is compared with those of the two-component

systems ZnPc-SubPc **8** and (BBPA)₃-ZnPor-ZnPc **9**, on one hand, and the single-component systems ZnPc **6** and F₁₂SubPc **11** (Figure 1), on the other hand. Despite the overall complexity of the multi-chromophoric arrays, it is possible to identify the signals corresponding to the protons of the different subunits. In particular, for the transformation of **9** into **1**, we monitored the upfield shift of the protons of the ethynylphenol, as the oxygen is bound to the boron atom of the F₁₂SubPc.

Scheme 1. Synthesis of 8, 9, and 1^a



^aReagents and conditions: i) BF₃·OEt₂, EtOH, CHCl₃, r.t.; ii) DDQ, NEt₃, r.t., 8%; iii) Zn(OAc)₂, CH₂Cl₂/MeOH (3:1), r.t., 96%; iv) TBAF, THF, 0°C; v) 3-ethynylphenol, Pd(PPh₃)₄, CuI, THF/NEt₃ (3:1), 60°C, 60%; vi) F₁₂SubPc **7**, AgOTf, toluene, r.t.; vii) ZnPc **10**, DIPEA, reflux, 15%; viii) Pd₂(dba)₃, AsPh₃, THF/NEt₃ (2:1), 60°C, 82%; ix) F₁₂SubPc **7**, AgOTf, toluene, r.t.; x) (BBPA)₃-ZnPor-ZnPc **9**, DIPEA, reflux, 6%.

Electrochemical Characterization. To determine the redox chemistry of **1**, in general, and its ability to power a cascade of charge transfer steps, in particular, we turned to electrochemical investigations. To this end, we probed reductive and oxidative processes with the single-, two-, three- and four-component systems. In Figure S14, the cyclic voltammograms (CV) of the individual components used as references, namely (BBPA)₃-ZnPor **5** and ZnPc **10**, are compared to that of **1**. The electrochemical behaviour of F₁₂SubPc **7** has been previously described.⁴⁵ On the reductive side, the first reductions of (BBPA)₃-ZnPor **5**, ZnPc **10**, and F₁₂SubPc **7** at -1.51, -1.18, and -1.10 V versus Fc/Fc⁺, respectively, are either quasi-reversible or reversible. On the oxidative side, the first oxidations of ZnPc **10** at +0.4 V vs Fc/Fc⁺ and that of F₁₂SubPc **7** at +0.46 V are reversible. In contrast, oxidation of (BBPA)₃-

ZnPor **5** occurs over a wide potential range, that is, from +0.3 to +0.9 V vs Fc/Fc⁺. A likely rationale implies that, next to a ZnPor centered oxidation, additional oxidations takes place at the BBPA units, as shown previously.^{46,47} The two-component reference system ZnPc-SubPc **8** (Figure S15), features a well-defined, ZnPc-centered oxidation at +0.39 V, and three reversible reductions at -1.04, -1.40 and -1.65 V, among which the first one involves F₁₂SubPc. Next, for the three-component ensemble (BBPA)₃-ZnPor-ZnPc **9** (Figure S16), the oxidations and reductions are consistent with those registered for the corresponding individual components **5** and **10**. Also in this case, the oxidation appears rather broad in the CV and comprises oxidation of the BBPA, ZnPor, and ZnPc. Deconvolution of the oxidative broad wave (Figure S16) allows to discern the ZnPor- and ZnPc-centered oxidation processes at +0.30 V and +0.39 V, respectively. The ZnPc and ZnPor reductions are well separated from each other and occur at -1.17 and -1.37 V, respectively.

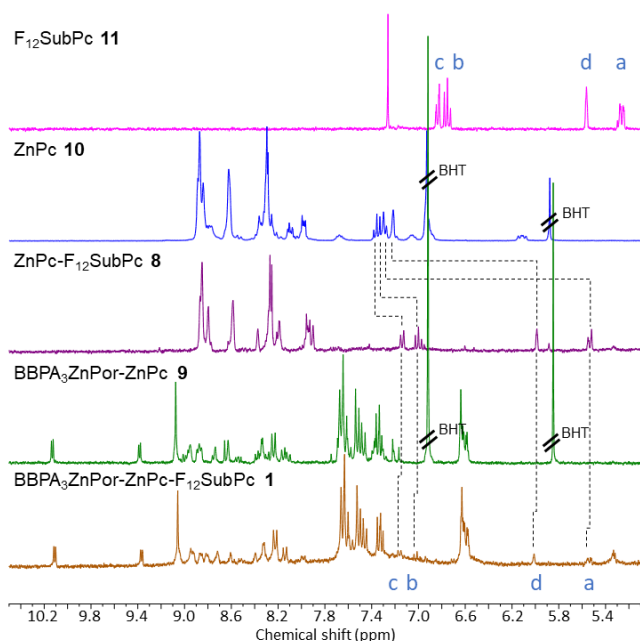
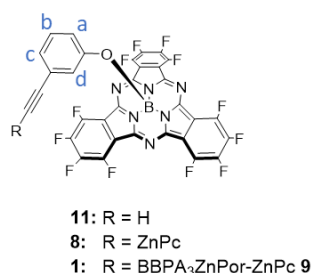


Figure 1. Comparison of ^1H -NMR spectra of **11** in CDCl_3 and **1**, **8**, **9**, and **10** in THF-d_8 . Dashed lines are drawn to guide the eye to the changes in the chemical shifts of protons Ha, Hb, Hc and Hd.

In the final ensemble **1**, the corresponding reductions and oxidations are also in sound agreement with those recorded for the single- and two-component references. In Table 1, all the redox values, which were either registered for **1**, **5**, **8**, **9** and **10**, or taken for $\text{F}_{12}\text{SubPc}$ **7** from the literature,⁴⁵ are compiled. With the electrochemical data of each system at hands, we calculated the energies of the charge-separated states in $(\text{BBPA})_3\text{-ZnPor-ZnPc}$ **9**, ZnPc-SubPc **8**, and $(\text{BBPA})_3\text{-ZnPor-ZnPc-SubPc}$ **1**. Moreover, upon considering the singlet excited state energies of $(\text{BBPA})_3\text{-ZnPor}$, ZnPc , and $\text{F}_{12}\text{SubPc}$, we gathered information regarding the driving forces for the initial charge separation. Those for the charge recombination came from the aforementioned energies of the charge-separated states and triplet excited state energies. Finally, the driving forces for a charge shift were taken from the differences of the charge-separated state energies.

Table 1. First oxidation and reduction for **1**, **5**, **7**, **8**, **9** and **10** extracted from square wave experiments.

Compound	$E_{\text{ox}}^{1/2} / \text{V vs Fc/Fc}^+$	$E_{\text{red}}^{1/2} / \text{V vs Fc/Fc}^+$
5	0.33 ^a	-1.51 ^c
7	1.00 ^b	-0.93 ^b
8	0.39 ^c	-1.04 ^d
9	0.30 ^e	-1.17 ^d
10	0.40 ^d	-1.18 ^d
1	0.36 ^c	-1.10 ^c

^a Shoulder. ^b Literature data. ^c Quasi-reversible. ^d Reversible. ^e Obtained from deconvolution of the broad oxidative process.

Photophysical Characterization of Individual Components. We first turned our attention to the individual components, that is, $(\text{BBPA})_3\text{-ZnPor}$ **5**, $\text{F}_{12}\text{SubPc}$ **11** (Figure 1), and ZnPc **10**. Based on a ground state absorption spectrum of $(\text{BBPA})_3\text{-ZnPor}$ **5** in toluene (Figure S17), in which Soret and Q-band transitions are discernable at 445 nm and at 558, 602 nm, respectively, 430 nm photoexcitation was selected for the fs-TAS. The instantaneous population of the second singlet excited state with characteristic features at 486 and 782 nm is accompanied by a ground state bleaching at 448 nm (Figure S19). A 0.5 ps ($2.0 \times 10^{12} \text{ s}^{-1}$) lasting internal conversion is the predominant fate of the second singlet excited state and, in turn, leads to the formation of the first singlet excited state. Major singlet excited state features for $(\text{BBPA})_3\text{-ZnPor}$ **5** are maxima at 487 and 580 nm, and minima at 448, 560 and 617 nm. The fluorescence maximizes at 619 nm (Figure S18) with an underlying fluorescence quantum yield of 0.086. The strongly fluorescent first singlet excited state transforms with 1.6 ns ($6.2 \times 10^8 \text{ s}^{-1}$) via intersystem crossing into to the poorly phosphorescent and long-lived triplet excited state. For **5**, the spectral characteristics of the triplet excited state include new maxima at 480 and 810 nm.

In $\text{F}_{12}\text{SubPc}$ **11**, the absorption spectrum in toluene features a Soret and a Q-band transition at 304 and 572 nm, respectively (Figure S20). Accordingly, we used in fs-TAS 550 nm photoexcitation, which resulted in the prompt formation of the first singlet excited state (Figure S21). Here, the most notable features are maxima at 430 and 786 nm, as well as minima at 517, 573 and 632 nm. On a timescale of 1.9 ns ($5.3 \times 10^8 \text{ s}^{-1}$), the triplet excited state of SubPc emerges and replaces the strongly fluorescent singlet excited state, for which a quantum yield of 0.17 was determined.⁴⁸ The presence of the correspondingly formed triplet excited state is corroborated by maxima at 450 and 615 nm, as well as minima at 530 and 570 nm.

In ZnPc **10**, all of the aforementioned absorption and fluorescence features are red-shifted relative to **5** and **11**. For example, the Soret and Q-band transitions are discernable in toluene at 356, as well as 680 and 705 nm, respectively (Figure S22), while the fluorescence maximizes with a quantum yield of 0.10 at 710 nm (Figure S23). For ZnPc **10**, 676 nm photoexcitation was selected for the fs-TAS measurements and the directly formed singlet excited state reveals maxima at 455, 635, 660, 760, and 822 nm and minima at 615, 647, 680, 710, and 796 nm in toluene (Figure S24). This is followed by an

intersystem crossing of 1.3 ns ($7.6 \times 10^8 \text{ s}^{-1}$), which affords the simultaneous formation of a prominent maximum at 486 nm, accompanied by maxima at 600, 632, and 660 nm, as well as minima at 620, 648, and 708 nm. All of the latter features are assigned to the long-lived triplet excited state of **10**.

Photophysical Characterization of Two-Component System.

When turning to ZnPc–SubPc **8** in toluene, its absorption spectrum reveals Soret band transitions at 310 nm from SubPc and at 349 nm from ZnPc, as well as Q-band transitions at 573 nm from SubPc and at 676 / 706 nm, accompanied by shoulders at 612 / 645 nm, from ZnPc (Figure S25). Notably, these values are similar to the values determined for the individual components – vide supra. In **8**, the relative intensities / extinction coefficients are also in sound agreement with those of ZnPc and SubPc, which points to a lack of ground state interactions.

From steady-state fluorescence measurements, we conclude that the SubPc fluorescence is strongly quenched and that its fluorescence quantum yield is 0.014 relative to a value of 0.17 seen for F₁₂SubPc **11**. Evidence for an intramolecular energy transfer came from ZnPc fluorescence quantum yields, which are as high as 0.22, upon, however, exciting SubPc (Figure S26). Relative to ZnPc **10**, the ZnPc fluorescence quantum yield in **8** – 0.10 versus 0.30 in toluene upon exciting – prompts to an additional deactivation pathway. An increase in solvent polarity has no impact on the SubPc fluorescence quantum yields, but lowers the ZnPc fluorescence quantum yields to 0.037. In other words, we postulate a charge transfer evolving from the ZnPc singlet excited state.

Due to the overall weak SubPc absorptions in ZnPc–SubPc **8**, the focus of fs-TAS was only placed on the excitation of ZnPc. The resulting data were fitted by Global analysis to a sequential three or four species kinetic model in toluene or anisole and benzonitrile, respectively shown in Figure S27. To this end, 676 nm photoexcitation of **8** is associated with the ZnPc singlet excited state (1.58 eV) formation. This is the second species and reveals maxima at 465, 598, 633, 659, 761, 826, and 983 nm and minima at 617, 646, 681 and 706 nm.⁴⁹ All of them are formed promptly. In toluene, the ZnPc singlet excited state undergoes a fast and 4 ps ($2.5 \times 10^{11} \text{ s}^{-1}$) lasting vibrational relaxation, followed by a slow intersystem crossing, which takes 1.7 ns ($5.9 \times 10^8 \text{ s}^{-1}$) to populate the ZnPc triplet excited state (Figure S28). Most notable are the following fingerprints: a maximum at 486 nm as well as minima at 620, 648, and 708 nm.

Turning towards more polar solvents, instead of the slow intersystem crossing, a fast decay dominates the photoexcited state reactivity of with the ZnPc singlet excited state (Figures 2 and S29). Important is in this context that we identified, on one hand, the one-electron oxidized form of ZnPc, with its broad transient around 840 nm, and on the other hand, the one-electron reduced form of SubPc with a maximum at 504 nm and ground-state bleaching at 578 nm. These features resemble those well, which are found in the literature.⁵⁰ In **8**, next to the formation of the ZnPc^{•+}–SubPc^{•–} charge-separated state (1.32 eV) as the third species, the photoexcited ZnPc might transform as well into the ZnPc^{•–}–SubPc^{•+} charge-separated state (2.28 eV). Considering that the earlier process is exergonic by about 0.3 eV and the latter is endergonic by about 0.7 eV the earlier dominates over the latter. When comparing different solvent polarities, such as anisole and benzonitrile, charge separation and charge recombination were determined as 478 ps ($2.09 \times 10^9 \text{ s}^{-1}$) / 46 ps ($2.16 \times 10^{10} \text{ s}^{-1}$), and 2500 ps ($2.00 \times 10^8 \text{ s}^{-1}$) /

414 ps ($2.41 \times 10^9 \text{ s}^{-1}$), respectively. The final product of this sequence is, in all solvents, the ZnPc triplet excited state as the fourth species.

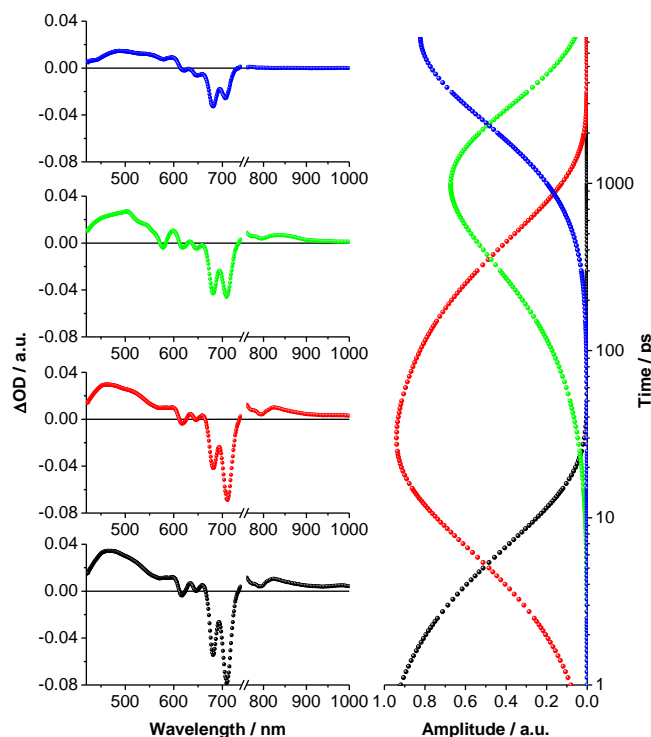


Figure 2. Left: Evolution-associated transient absorption difference spectra of 1*ZnPc–SubPc (black; $1.46 \times 10^{11} \text{ s}^{-1}$), 1*ZnPc–SubPc (red; $2.09 \times 10^9 \text{ s}^{-1}$), ZnPc^{•+}–SubPc^{•–} (green; $2.00 \times 10^8 \text{ s}^{-1}$), and 3*ZnPc–SubPc (blue; $2.0 \times 10^4 \text{ s}^{-1}$) for **8** ($2.5 \times 10^{-5} \text{ M}$) as obtained by global analysis for a four species kinetic model that is shown in Figure S36. Right: Associated time-dependent amplitudes. Data were obtained upon fs-TAS (676 nm, 200 nJ) in argon-saturated anisole.

Photophysical Characterization of Three-Component System.

Next, the three-component system, namely **9**, was probed. The absorption spectrum of (BBPA)₃–ZnPc–ZnPor **9** in toluene deviates from the linear superimposition of the absorption spectra of the individual components. On one hand, the (BBPA)₃–ZnPc Soret and Q-band transitions evolve at 451 and 572 nm, respectively, and those of ZnPc are discernable at 331 and 710 nm (Figure S30). On the other hand, the intensities / extinction coefficients are altered and the transitions are broadened in **9** relative to **5** and **10**. All of the aforementioned suggest appreciable ground state interactions mediated by the ethynyl-bridge.

Notable are also the interactions in the excited state. From steady-state fluorescence measurements (Figure S31) we derive that the ZnPor fluorescence with a quantum yield of 0.008 is strongly quenched relative to 0.086 seen in (BBPA)₃–ZnPc **5**, which is indicative of either an intramolecular energy or charge transfer. In addition, a low ZnPc fluorescence quantum yield of 0.015 rather than 0.3 in ZnPc **10** suggests yet another deactivation process, that is, a charge transfer. Evidence for the charge transfer stems from the fact that changes in solvent polarity affect the ZnPc fluorescence quantum yields in the form of an overall lowering.

To shed light onto the ZnPc fluorescence quenching we probed (BBPA)₃–ZnPc–ZnPor **9** in fs-TAS experiments following 676 nm photoexcitation. A four species kinetic model, which is shown in

Figure S32, was implemented to fit the corresponding data by means of Target analysis. Right after the conclusion of the laser pulse in anisole, the ZnPc singlet excited state (1.58 eV) with maxima at 513 and 605 nm as well as minima at 456 and 716 nm is populated as the first species (Figure 3). Due to the strong coupling between (BBPA)₃-ZnPor and ZnPc via the ethynyl-bridge, the ZnPc singlet excited state transforms within 13 ps ($7.7 \times 10^{10} \text{ s}^{-1}$) into the second species, that is, a delocalized excited state. The latter is characterized by an intensification of the (BBPA)₃-ZnPor Soret band bleaching at 454 nm, a minimum at 716 nm, and a maximum at 595 nm. Hand-in-hand with its 100 ps ($1.00 \times 10^{10} \text{ s}^{-1}$) decay is the simultaneous growth of newly developing maxima at 470 and 785 nm, as well as a hypsochromically shifted ground state bleaching at 440 nm, which are attributed to the formation of the one-electron oxidized form of (BBPA)₃-ZnPor. In addition, we note the simultaneously evolving transient at 660 nm. The latter is assigned to the one-electron reduced form of ZnPc and, in turn, we imply the formation of the (BBPA)₃-ZnPor^{•+}-ZnPc^{•-} charge-separated state (1.57 eV) as the third species.⁵¹ On longer timescales, the (BBPA)₃-ZnPor^{•+}-ZnPc^{•-} charge-separated state is subject to a charge shift; within 179 ps ($5.58 \times 10^9 \text{ s}^{-1}$), the (BBPA)₃-ZnPor^{•+}-ZnPc^{•-} charge-separated state transforms into a (BBPA)₃-ZnPor-ZnPc^{•-} charge-separated state. The (BBPA)₃-ZnPor-ZnPc^{•-} charge-separated state is the fourth species. Evidence for the underlying shift of charge from ZnPor to BBPA comes from the decay of the ZnPor ground state bleaching and the slight 600 nm fingerprint of the one-electron oxidized form of BBPA. The remaining transients are the ZnPc ground state bleaching at 714 nm as well as a slight maximum at 486 nm, which are attributed to the ZnPc triplet excited state. In complementary ns-TAS experiments the ZnPc triplet excited state was identified as the final product of charge recombination.

A change in polarity from toluene via anisole to benzonitrile impacts the excited state dynamics with 12 ($8.4 \times 10^{10} \text{ s}^{-1}$), 13 ($7.7 \times 10^{10} \text{ s}^{-1}$), and 8 ps ($1.3 \times 10^{11} \text{ s}^{-1}$) for population of the delocalized excited state, 202 ($4.96 \times 10^9 \text{ s}^{-1}$), 100 ($1.00 \times 10^{10} \text{ s}^{-1}$), and 20 ps ($5.1 \times 10^{10} \text{ s}^{-1}$) for charge separation, 990 ($1.01 \times 10^9 \text{ s}^{-1}$), 179 ($5.58 \times 10^9 \text{ s}^{-1}$), and 63 ps ($1.58 \times 10^9 \text{ s}^{-1}$) for charge shift and 15 ($6.7 \times 10^7 \text{ s}^{-1}$), 9 ($1.1 \times 10^8 \text{ s}^{-1}$), and 9 ns ($1.1 \times 10^8 \text{ s}^{-1}$) for charge recombination to the ZnPc triplet excited state, respectively (Figures S33-S35).

Photophysical Characterization of Four-Component System. In the final step, we performed ground and excited state investigations with (BBPA)₃-ZnPor-ZnPc-SubPc **1**. Its absorption spectrum in toluene features like (BBPA)₃-ZnPor-ZnPc **9** and ZnPc-SubPc **8** the Soret and Q-band transitions of (BBPA)₃-ZnPor **5**, ZnPc **10**, and F₁₂SubPc **11** (Figure S36). Analyses of the Q-band transitions at 710 and 573 nm, which reveal broadening relative to those of SubPc and ZnPc, respectively, confirm the presence of electronic interactions between the individual components.

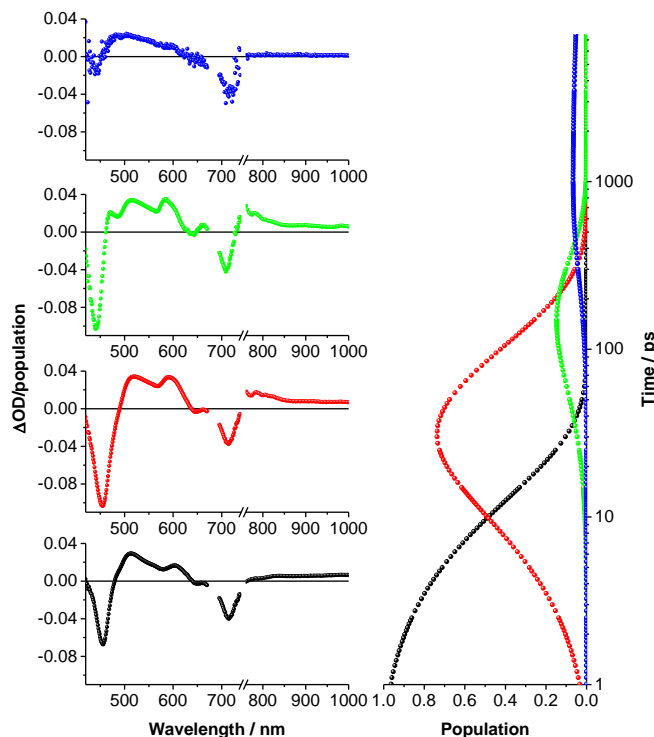


Figure 3. Left: Deconvoluted species-associated transient absorption difference spectra of (BBPA)₃-ZnPor^{•+}*(ZnPc) (black; $7.7 \times 10^{10} \text{ s}^{-1}$), (BBPA)₃-(ZnPor-ZnPc)* (red; $1.00 \times 10^{10} \text{ s}^{-1}$), (BBPA)₃-ZnPor^{•+}-ZnPc^{•-} (green; $5.58 \times 10^9 \text{ s}^{-1}$), and (BBPA)₃^{•+}-ZnPor-ZnPc^{•-} (blue; $1.1 \times 10^8 \text{ s}^{-1}$) for **9** ($2.5 \times 10^{-5} \text{ M}$) as obtained by target analysis for a four species kinetic model that is shown in Figure S37. The kinetic model is solely based on fs-TAS measurements without accounting for the ns-TAS data. The (BBPA)₃-ZnPor-ZnPc^{•-} quantum yield is 7%. Right: Population kinetics for each species. Data were obtained upon fs-TAS (676 nm, 200 nJ) in argon-saturated anisole.

We first conducted fs-TAS experiments in anisole, with 676 nm photoexcitation to excite ZnPc quantitatively (Figure 4).⁵² The best fits of the experimental data were obtained by applying Target Analysis involving a five species kinetic model (Figure S37). The first species is the ZnPc singlet excited state, which is formed initially with its characteristic maxima at 513, 602, and 983 nm and minima at 457 and 720 nm. It is rather short-lived and its decay is with 7.8 ps ($1.3 \times 10^{11} \text{ s}^{-1}$) similar to what has been seen for (BBPA)₃-ZnPor-ZnPc **9**. As such, it is associated with the formation of the second species in the form of the delocalized excited state. Characteristics are an intensified ground state bleaching at 456 nm and a new transient at 600 nm. The subsequent hypsochromic shift from 456 to 444 nm, as well as the growth of a new transient at 785 nm are attributed to the formation of the one-electron oxidized form of ZnPor. This happens with 67 ps ($1.2 \times 10^{10} \text{ s}^{-1}$), from which we conclude the formation of the third species. Besides the aforementioned, the prominent maxima at 592 and 808 nm are indicative of the one-electron reduced form of ZnPc, which implies the formation of a (BBPA)₃-ZnPor^{•+}-ZnPc^{•-}-SubPc charge-separated state (1.57 eV). The latter is followed by a 83 ps charge shift ($1.5 \times 10^{10} \text{ s}^{-1}$) and yields, in turn, the fourth species, namely the (BBPA)₃-ZnPor^{•+}-ZnPc-SubPc^{•-} charge-separated state (1.32 eV). Corroboration for the charge shift comes from bleaching of the SubPc ground state at 578 nm, as well as a maximum at 507 nm. Both are indicators of the presence of the one-electron reduced form of SubPc. Importantly, while SubPc^{•-} is persistent, ZnPor^{•+} is found to decay; its 1.4 ns ($7.2 \times 10^8 \text{ s}^{-1}$)

decay is linked kinetically to the growth of one-electron oxidized form of BBPA with its 600 nm fingerprint and leads, in turn, to the final formation of $(\text{BBPA})_3^{+*}\text{-ZnPc-SubPc}^{*-}$ (~ 1.5 eV) as the fifth species.⁵³ Its formation is followed by a 10.0 ns ($1.00 \times 10^8 \text{ s}^{-1}$) charge recombination. In benzonitrile, charge delocalization is 4.3 ps ($2.3 \times 10^{11} \text{ s}^{-1}$), charge separation is 30 ps ($3.2 \times 10^{10} \text{ s}^{-1}$), charge shift to SubPc is 31 ps ($3.3 \times 10^{10} \text{ s}^{-1}$), charge shift from BBPA to ZnPc is 311 ps ($3.22 \times 10^9 \text{ s}^{-1}$), and charge recombination is 11.2 ns ($8.93 \times 10^7 \text{ s}^{-1}$) (Figure S38).

In ns-TAS experiments, the final product of this sequence is the ZnPc triplet excited state with a lifetime of 40 μs ($2.5 \times 10^4 \text{ s}^{-1}$). Among all the chromophores, that is, ZnPc, ZnPc, and SubPcs, the ZnPc triplet is the lowest in energy and characterized by a ZnPc ground state bleaching at 714 nm as well as a maximum at 486 nm.

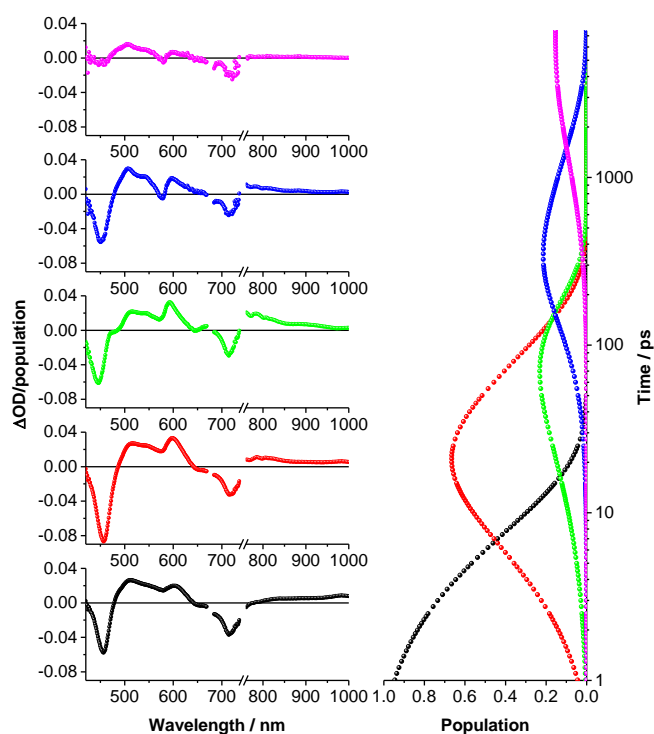


Figure 4. Left: Deconvoluted species-associated transient absorption difference spectra of $\text{BBPA}_3\text{-ZnPc-SubPc}$ (black; $1.3 \times 10^{10} \text{ s}^{-1}$), $\text{BBPA}_3\text{-(ZnPc-ZnPc)*-SubPc}$ (red; $1.2 \times 10^{10} \text{ s}^{-1}$), $\text{BBPA}_3\text{-ZnPc*+ZnPc*-SubPc}$ (green; $1.5 \times 10^{10} \text{ s}^{-1}$), $\text{BBPA}_3\text{-ZnPc*+ZnPc*-SubPc}$ (blue; $7.2 \times 10^8 \text{ s}^{-1}$), and $\text{BBPA}_3^{+*}\text{-ZnPc-ZnPc-SubPc}^{*-}$ (magenta; $1.00 \times 10^8 \text{ s}^{-1}$) for **1** ($2.5 \times 10^{-5} \text{ M}$) as obtained by target analysis for a five species kinetic model that is shown in Figure S40. The $(\text{BBPA})_3\text{-ZnPc-ZnPc-SubPc}^{*-}$ quantum yield is 14%. The kinetic model is solely based on fs-TAS measurements without accounting for the ns-TAS data. Right: Population kinetics for each species. Data were obtained upon fs-TAS (676 nm, 200 nJ) in argon-saturated anisole.

Conclusions

We have successfully prepared a panchromatic electron donor-acceptor conjugate (**1**) comprising three porphyrinoid chromophores, that is, a BBPA-functionalized ZnPc, ZnPc and SubPc. The combination of the three porphyrinoids in a covalent $(\text{BBPA})_3\text{-ZnPc-ZnPc-SubPc}$ conjugate follows a rational design towards an appropriate energy level alignment, and, in turn, a cascade of energy and charge transfer processes. To that end, ZnPc serves, after photoexcitation, as primary electron donor on account of its functionalization with three electron-donating

BBPA, which, in turn, play the role of secondary electron donors, and which assist in stabilizing the final charge-separated state. On the other hand, a perfluorinated SubPc is included as the constituent with the lowest LUMO energy. Finally, ZnPc is positioned as central unit and operates as energy/electron transfer funnel between the ZnPc and the SubPc termini. Our unique conjugate meets the requirements needed to power the formation of a long-lived charge-separated state once photoexcited. As a matter of fact, after photoexcitation of the central ZnPc component, the formation of $(\text{BBPA})_3\text{-ZnPc*+ZnPc*-SubPc}$ charge-separated state was followed by a charge shift from ZnPc to SubPc, and from ZnPc to the BBPA units, to afford the $(\text{BBPA})_3^{+*}\text{-ZnPc-ZnPc-SubPc}^{*-}$ charge-separated state. The panchromatic character of **1**, together with its cascade-like charge transfer behaviour prove this ensemble a unique photosynthetic reaction center mimic.

Conflicts of interest

There are no conflicts to declare.

Author information

Corresponding Author

*gema.delatorre@uam.es

*dirk.guldi@fau.de

*tomas.torres@uam.es

Gema de la Torre ORCID ID 0000-0002-4585-974

Dirk M. Guldi ORCID ID 0000-0002-3960-1765

Tomas Torres ORCID ID 0000-0001-9335-6935.

Author Contributions

The manuscript was written through contributions of all authors. / All authors have given approval to the final version of the manuscript.

Funding Sources

Financial support from Comunidad de Madrid, Spain (S2013/MIT-2841, FOTOCARBON), and MINECO, Spain (CTQ2017-85393-P), and the "Solar Energy goes Hybrid" Initiative of the Bavarian Ministry for Science, Culture and Education (SolTech) is acknowledged.

Abbreviations

ZnPc, zinc(II) phthalocyanine; ZnPc, zinc(II) porphyrin; SubPc, subphthalocyanine; BBPA, bis(biphenyl)phenylamine; TAS, transient absorption spectroscopy

Notes and references

- 1 B Alberts, A. Johnson, J. Lewis, D. Morgan, M. Raff, K. Roberts and P. Walter, *Molecular Biology of the Cell*; 500 Tips; Garland Science, 2014.
- 2 L. Hammarstrom, *Acc. Chem. Res.* 2015, **48**, 840.
- 3 D. Gust, *Nature* 1997, **386**, 21.

- 4 *Electron Transfer in Chemistry*; V. Balzani, Ed.; Wiley-VCH: Weinheim, Germany, 2001; Vols. 1-4.
- 5 D. M. Guldi, *Chem. Soc. Rev.* 2002, **31**, 22.
- 6 H. Imahori, Y. Mori, Y. Matano, *J. Photochem. Photobiol. C* 2003, **4**, 51.
- 7 S. Fukuzumi, *Phys. Chem. Chem. Phys.* 2008, **10**, 2283.
- 8 M. R. Wasielewski, *Acc. Chem. Res.* 2009, **42**, 1910.
- 9 D. Gust, T. A. Moore, A. L. Moore, *Acc. Chem. Res.* 2009, **42**, 1890.
- 10 G. N. Lim, E. Maligaspe, M. E. Zandler, F. D'Souza, *Chem. Eur. J.* 2014, **20**, 17089.
- 11 M. Fathalla, J. C. Barnes, R. M. Young, K. J. Hartlieb, S. M. Dyar, S. W. Eaton, A. A. Sarjeant, D. T. Co, M. R. Wasielewski, J. F. Stoddart, *Chem. – A Eur. J.* 2014, **20**, 14690.
- 12 P. K. Poddutoori, L. P. Bregles, G. N. Lim, P. Boland, R. G. Kerr, F., D'Souza *Inorg. Chem.* 2015, **54**, 8482.
- 13 A. S. Konev, A. F. Khlebnikov, P. I. Prolubnikov, A. S. Mereshchenko, A. V. Povolotskiy, O. V. Levin, A. Hirsch, *Chem. – A Eur. J.* 2015, **21**, 1237.
- 14 G. de la Torre, C. G. Claessens, T. Torres, *Chem. Commun.* 2007, 2000.
- 15 G. Bottari, G. de la Torre, D. M. Guldi, T. Torres, *Chem. Rev.* 2010, **110**, 6768.
- 16 H. Imahori, T. Umeyama, K. Kurotobi, Y. Takano, *Chem. Commun.* 2012, **48**, 4032.
- 17 G. de la Torre, G. Bottari, T. Torres, *Adv. Energy Mater.* 2016, 1601700.
- 18 C. G. Claessens, D. González-Rodríguez, T. Torres, *Chem. Rev.* 2002, **102**, 835.
- 19 C. G. Claessens, D. González-Rodríguez, M. S. Rodríguez-Morgade, A. Medina, T. Torres, *Chem. Rev.* 2014, **114**, 2192.
- 20 G. Bottari, G. de la Torre, D. M. Guldi, T. Torres, In *Multiporphyrin Arrays*; Pan Stanford Publishing, 2012; pp 149–216.
- 21 P.-C. Lo, X. Leng, D. K. P. Ng, *Coord. Chem. Rev.* 2007, **251**, 2334.
- 22 J.-Y. Liu, P.-C. Lo, D. K. P. Ng, In *Functional Phthalocyanine Molecular Materials*; J. Jiang, Ed.; Springer Berlin Heidelberg: Berlin, Heidelberg, 2010; pp 169–209.
- 23 G. de la Torre, G. Bottari, M. Sekita, A. Hausmann, D. M. Guldi, T. Torres, *Chem. Soc. Rev.* 2013, **42**, 8049.
- 24 A. Ambroise, R. W. Wagner, P. D. Rao, J. A. Riggs, P. Hascoat, J. R. Diers, J. Seth, R. K. Lammi, D. F. Bocian, D. Holten, J. S. Lindsey, *Chem. Mater.* 2001, **13**, 1023.
- 25 A. M. V. M. Pereira, A. Hausmann, J. P. C. Tome, O. Trukhina, M. Urbani, M. G. P. S. Neves, J. A. S. Cavaleiro, D. M. Guldi, T. Torres, *Chem. Eur. J.* 2012, **18**, 3210.
- 26 M. E. El-Khouly, D. K. Ju, K.-Y. Kay, F. D'Souza, S. Fukuzumi, *Chem. – A Eur. J.* 2010, **16**, 6193.
- 27 R. F. Enes, J.-J. Cid, A. Hausmann, O. Trukhina, A. Gouloumis, P. Vázquez, J. A. S. Cavaleiro, A. C. Tomé, D. M. Guldi, T. Torres, *Chem. – A Eur. J.* 2012, **18**, 1727.
- 28 Y. Rio, W. Seitz, A. Gouloumis, P. Vázquez, J. L. Sessler, D. M. Guldi, T. Torres, *Chem. Eur. J.* 2010, **16**, 1929.
- 29 Ch. B. KC, G. N. Lim, F. D'Souza, *Nanoscale*, 2015, **7**, 6813.
- 30 L. Martín-Gomis, F. Peralta-Ruiz, M. B. Thomas, F. Fernández-Lázaro, F. D'Souza, A. Sastre-Santos, *Chem. Eur. J.* 2017, **23**, 3863.
- 31 M. García-Iglesias, K. Peuntinger, A. Kahnt, J. Krausmann, P. Vázquez, D. González-Rodríguez, D. M. Guldi, T. Torres, *J. Am. Chem. Soc.* 2013, **135**, 19311.
- 32 R. Menting, J. T. F. Lau, H. Xu, D. K. P. Ng, B. Roder, E. A. Ermilov, *Chem. Commun.* 2012, **48**, 4597.
- 33 C. A. Wijesinghe, M. E. El-Khouly, M. E. Zandler, S. Fukuzumi, F. D'Souza, *Chem. – A Eur. J.* 2013, **19**, 9629.
- 34 H. Gommans, T. Aernouts, B. Verreert, P. Heremans, A. Medina, C. G. Claessens, T. Torres, *Adv. Funct. Mater.* 2009, **19**, 3435.
- 35 B. Verreert, J. Cnops, D. Cheyns, P. Heremans, A. Stesmans, G. Zango, C. G. Claessens, T. Torres, B. P. Rand, *Adv. Energy Mater.* 2014, **4**, 1301413.
- 36 K. M. Mullen, I. H. M. van Stokkum, *J. Stat. Softw.* 2007, **18**, 1.
- 37 J. J. Snellenburg, S. P. Liptonok, R. Seger, K. M. Mullen, I. H. M. van Stokkum *J. Stat. Softw.* 2012, **49**, 1.
- 38 P. Gao, Y. J. Kim, J.-H. Yum, T. W. Holcombe, M. K. Nazeeruddin, M. Grätzel, *J. Mater. Chem. A* 2013, **1**, 5535.
- 39 J. S. Lindsey, I. C. Schreiman, H. C. Hsu, P. C. Kearney, A. M. Marguerettaz, *J. Org. Chem.* 1987, **52**, 827.
- 40 J. S. Lindsey, K. A. MacCrum, J. S. Tyhonas, Y. Y. Chuang, *J. Org. Chem.* 1994, **59**, 579.
- 41 E. Fazio, J. Jaramillo-García, G. de la Torre, T. Torres, *Org. Lett.* 2014, **16**, 4706.
- 42 C. G. Claessens, D. González-Rodríguez, B. del Rey, T. Torres, G. Mark, H.-P. Schuchmann, C. von Sonntag, J. G. MacDonald, R. S. Nohr, *European J. Org. Chem.* 2003, **2003**, 2547.
- 43 J. Guilleme, D. González-Rodríguez, T. Torres, *Angew. Chem. Int. Ed.* 2011, **50**, 3506.
- 44 E. Fazio, J. Jaramillo-García, M. Medel, M. Urbani, M. Grätzel, M. K. Nazeerudin, G. de la Torre, T. Torres, *ChemistryOpen* 2017, **6**, 121.
- 45 R. S. Iglesias, C. G. Claessens, T. Torres, M. A. Herranz, V. R. Ferro, J. M. García de la Vega, *J. Org. Chem.* 2007, **72**, 2967.
- 46 B. Liu, W. Zhu, Y. Wang, W. Wu, X. Li, B. Chen, Y.-T. Long, Y. Xie, *J. Mater. Chem.* 2012, **22**, 7434.
- 47 M.-E. Ragoussi, G. de la Torre, T. Torres, *Eur. J. Org. Chem.* 2013, 2832.
- 48 L. Feng, M. Rudolf, O. Trukhina, Z. Slanina, F. Uhlik, X. Lu, T. Torres, D. M. Guldi, T. Akasaka, *Chem. Commun.* 2015, **51**, 330.
- 49 The first species is a higher lying ZnPc singlet excited state.
- 50 M. Rudolf, O. Trukhina, J. Perles, L. Feng, T. Akasaka, T. Torres, D. M. Guldi, *Chem. Sci.* 2015, **6**, 4141.
- 51 Based on the difficulty to record an accurate oxidation of ZnPor **5** we took the HOMO energy from the optical (E_{0-0}) bandgap obtained from the interception between the absorption and fluorescence spectra (Figure S18).
- 52 Please note that laser excitation was only conducted in anisole and benzonitrile due to the aforementioned lack of any charge separation in the ZnPc-SubPc dyad in toluene.
- 53 Oxidative potentials are obtained from related TPA described in M.-E. Ragoussi, G. de la Torre, T. Torres, *Eur. J. Org. Chem.* 2013, 2832.